nature physics

Article

https://doi.org/10.1038/s41567-024-02412-4

Leggett modes in a Dirac semimetal

Received: 24 June 2022

Accepted: 24 January 2024

Published online: 4 April 2024

Check for updates

Joseph J. Cuozzo[1,2,6] ✉, W. Yu[3,4,6], P. Davids[3], T. M. Nenoff[3], D. B. Soh[2,5], Wei Pan[2] ✉ & Enrico Rossi[1] ✉

Experiments have shown that several materials, including MgB_2, iron-based superconductors and monolayer $NbSe_2$, are multiband superconductors. Superconducting pairing in multiple bands can give rise to phenomena not available in a single band, including Leggett modes. A Leggett mode is the collective periodic oscillation of the relative phase between the phases of the superconducting condensates formed in the different bands. The experimental observation of Leggett modes is challenging because multiband superconductors are rare and because these modes describe charge fluctuations between bands and therefore are hard to probe directly. Also, the excitation energy of a Leggett mode is often larger than the superconducting gaps, and therefore they are strongly overdamped via relaxation processes into the quasiparticle continuum. Here, we show that Leggett modes and their frequency can be detected in a.c. driven superconducting quantum interference devices. We then use the results to analyse the measurements of such a quantum device, one based on a Dirac semimetal Cd_3As_2, in which superconductivity is induced by proximity to superconducting Al. These results show the theoretically predicted signatures of Leggett modes, and therefore we conclude that a Leggett mode is present in the two-band superconducting state of Cd_3As_2.

The superconducting state is well described by a complex order parameter $\Delta(\mathbf{r}) = |\Delta(\mathbf{r})|e^{i\phi(\mathbf{r})}$, characterized by an amplitude and a phase that, in general, depend on the position $\mathbf{r}$. The time dependence of $\Delta(\mathbf{r})$ describes the collective, low energy excitations of a superconductor. In a standard single-band superconductor there are two types of collective excitations: Anderson–Higgs modes, corresponding to fluctuations of $|\Delta|$ and pseudo-Goldstone modes, corresponding to fluctuations of the phase ϕ. The Fermi surface of a multiband metal is formed by several generally disconnected Fermi pockets. In this case, at low temperatures, the metal can become a multiband superconductor characterized by different order parameters Δ_i for different Fermi pockets[1–5], as shown schematically in Fig. 1a. It was pointed out[6] that a multiband superconductor will have additional collective modes corresponding to fluctuations of the phase difference between the order parameters of different Fermi pockets. So far, evidence of Leggett modes has been obtained only via direct spectroscopy techniques in MgB_2 (refs. 7–11) and, more recently, in an Fe-based superconductor[12]. Using an approach of limited applicability, it had been theorized that in Josephson junctions (JJs) in which one lead is formed by a single-band superconductor and the other by a two-band superconductor, signatures of a Leggett mode could be present[13].

Here we show, using a different method, how the presence of Leggett modes can be observed in JJs and in a.c.-driven superconducting quantum interference devices (SQUIDs) in which all the leads are formed from the same multiband superconducting material. This opens a new approach to the detection and characterization of Leggett modes. In addition, we show that measurements on SQUIDs based on the superconducting Dirac semimetal (DSM) Cd_3As_2 display the theoretically predicted unique signatures associated with the presence of a Leggett mode. This adds Cd_3As_2 to the list of the few materials exhibiting the presence of Leggett modes and points to the unusual multiband character of the superconducting state in this material and possibly more generally in DSMs.

For a two-band superconductor, the dynamics of the Leggett mode can be described by the effective Lagrangian

[1]Department of Physics, William & Mary, Williamsburg, VA, USA. [2]Sandia National Laboratories, Livermore, CA, USA. [3]Sandia National Laboratories, Albuquerque, NM, USA. [4]Present address: Gusu Laboratory of Materials, Suzhou, China. [5]Present address: College of Optical Sciences, University of Arizona, Tucson, AZ, USA. [6]These authors contributed equally: Joseph J. Cuozzo, W. Yu. ✉e-mail: jjcuozz@sandia.gov; wpan@sandia.gov; erossi@wm.edu

https://doi.org/10.1038/s41567-024-02412-4

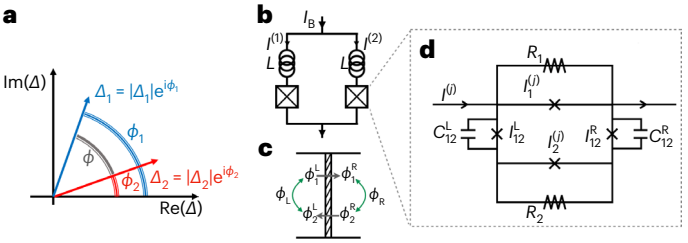

Fig. 1 | Leggett modes in SQUIDs. a, Schematic showing the relative phase ϕ between the two superconducting order parameters. **b**, SQUID circuit diagram. The boxes represent individual JJs, whose effective RCSJ model is shown in **d**. **c**, Diagram showing the superconducting phases across a JJ. **d**, Effective RCSJ model of individual JJ.

$$\mathcal{L} = (1/2)C_{12}(\hbar/2e)^2(\mathrm{d}\phi/\mathrm{d}t)^2 + (\hbar/2e)I_{12}\cos(\phi - \phi_0), \tag{1}$$

where $\hbar$ is the reduced Planck's constant, C_{12} is the interband capacitance, e is the electron's charge, I_{12} is the effective interband critical Josephson current[6] and ϕ_0 is the equilibrium value of ϕ. From equation (1) we obtain that when $\phi - \phi_0 \ll 1$, ϕ will oscillate with frequency $\omega_\mathrm{L} = \sqrt{(2e/\hbar)I_{12}/C_{12}}$ around ϕ_0.

A SQUID, see Fig. 1b, is formed by two JJs connected in parallel and encircling a finite size area. Let $\theta_i \equiv \phi_i^\mathrm{R} - \phi_i^\mathrm{L}$ be the difference between the superconducting order parameter in the right and left lead for band i. Then the current across the JJ's leads, for a JJ with low-medium transparency[14], is given by $I = I_1\sin(\alpha_1\theta_1) + I_2\sin(\alpha_2\theta_2)$ where I_i is the critical supercurrent for band i, and α_i is equal to 1 for a standard JJ and 1/2 for a topological JJ[15–17]. For biased high-transparency topologically trivial JJs, Landau–Zener transitions can induce a current–voltage response equivalent to a topological junction[18–20].

To understand the effect of a Leggett mode on the dynamics and voltage–current (V–I) characteristic of a JJ, we first present a simplified analysis of a voltage-biased JJ. A rigorous analysis of the realistic case of a current-biased JJ is presented later (see also Supplementary Section 1). The dynamics of the relative phase ϕ can induce oscillations in the phase difference $\psi \equiv (\theta_1 - \theta_2)/2$. Let $\phi_\mathrm{R} \equiv \phi_1^\mathrm{R} - \phi_2^\mathrm{R}$ and $\phi_\mathrm{L} \equiv \phi_1^\mathrm{L} - \phi_2^\mathrm{L}$, Fig. 1c, so that $\psi = (\phi_\mathrm{R} - \phi_\mathrm{L})/2 = \psi_0 + \tilde{\psi}(t)$, where ψ_0 is the equilibrium value of ψ and $\tilde{\psi}(t)$ the time dependent part. We can write $\theta_1 = \theta_\mathrm{A} + \psi$, $\theta_2 = \theta_\mathrm{A} - \psi$, with $\theta_\mathrm{A} = (\theta_1 + \theta_2)/2$. In the presence of a voltage V across the JJ's leads, we have $\mathrm{d}\theta_\mathrm{A}/\mathrm{d}t + \mathrm{d}\psi/\mathrm{d}t = 2eV/\hbar$. We consider the case when $V(t) = V_\mathrm{d.c.} + V_\mathrm{a.c.}\cos\omega t$. When the Leggett mode is driven, directly or indirectly, by a periodic drive, we can assume $\tilde{\psi} \approx \hat{A}_\omega\sin(\omega t)$, with $\hat{A}_\omega \approx A_0\Gamma_\mathrm{L}\omega/((\omega^2 - \omega_\mathrm{L}^2)^2 + \Gamma_\mathrm{L}^2\omega^2)$ the amplitude of the mode and Γ_L its broadening. In the limit when $\omega \approx \omega_\mathrm{L}$ so that $\hat{A}_{\omega_\mathrm{L}} \gg V_\mathrm{a.c.}/\omega$ we obtain:

$$\begin{aligned} I = \sum_{n=0}^{\infty}(-1)^n\Big[&I_1 J_n(\alpha_1(2e/\hbar)V_\mathrm{a.c.}/\omega_\mathrm{L}) \\ &\sin(\theta_0 + \psi_0 + \alpha_1(2e/\hbar)V_\mathrm{d.c.}t - n\omega_\mathrm{L}t) + \\ &(-1)^n I_2 J_n(\alpha_2 2\hat{A}_{\omega_\mathrm{L}})\sin(\theta_0 - \psi_0 + \alpha_2(2e/\hbar)V_\mathrm{d.c.}t - n\omega_\mathrm{L}t)\Big] \end{aligned} \tag{2}$$

where $J_n(x)$ is the nth Bessel function of the first kind. When $\alpha_1 = \alpha_2 = 1$, depending on the value of ψ_0, we can have suppression of the odd or even Shaprio spikes[19]. For $\psi_0 = 0$, we have suppression of the odd steps. In this case, for $\omega \approx \omega_\mathrm{L}$ the Shapiro steps' structure is qualitatively the same as the one obtained at low frequencies and powers in the presence of a topological superconducting channel ($\alpha_1 = \alpha_2 = 1/2$), or Landau–Zener processes in highly transparent junctions[18]. For small ω_L and non-negligible Γ_L, it might be difficult to pinpoint reliably the cause of the missing odd Shapiro steps. However, for the case when $\psi_0 = \pi/2$, equation (2) leads to a suppression of the even Shapiro spikes, a phenomenon that cannot be attributed to the topological nature of the JJ or to Landau–Zener processes. In the remainder, we assume $\alpha_1 = \alpha_2 = 1$ and discuss a concrete situation when we can expect $\psi_0 \neq 0$.

To describe the dynamics of an a.c.-current-biased 2-band JJ, we use a resistively and capacitively shunted junction (RCSJ) model[21,22]. When placing a lead on the surface of a DSM, the states of the lead couple strongly to the DSM's surface states and weakly to the DSM's bulk states. In this situation, the supercurrent in the bulk band (band 2) is mediated by interband processes (Fig. 1d), and a non-zero ψ_0 is expected. In particular, we expect $\phi_\mathrm{L} = \pi/2$ and $\phi_\mathrm{R} = -\pi/2$ so that $\psi_0 = \pi/2$. In this scenario, the values of ϕ_L and ϕ_R are not accidental but are the result of self-tuning in JJs based on DSMs in which superconductivity is induced via the proximity effect by a superconductor placed on the surface of the DSM. In this case, the current's lowest energy path to the bulk is via a Josephson supercurrent, $I_{12}^{(\mathrm{s})}$, between the surface band and the bulk band. Considering that in general for a JJ, we have the current–phase relation $I^{(\mathrm{s})} \propto \sin(\phi)$, we see that to maximize the supercurrent between surface and bulk the system will self-tune in a state in which on the left lead $\phi_\mathrm{L} = \pi/2$ and on the right lead $\phi_\mathrm{R} = -\pi/2$, given that on the right lead $I_{12}^{(\mathrm{s})}$ has to flow in the opposite direction, from bulk to surface, Fig. 1d (see also Supplementary Fig. 1 and Supplementary Section 1). The capacitance between the two leads is very small compared to the normal resistances R_i across the leads, so it can be neglected. Conversely, for the interband charge flow within the same lead, we can neglect the resistive channel, considering the non-negligible interband capacitance C_{12}. The resulting effective RCSJ model is shown in Fig. 1d.

In the presence of the current bias $I_\mathrm{B} = I_\mathrm{d.c.} + I_\mathrm{a.c.}\cos(\omega t)$, the dynamics of the RCSJ model shown in Fig. 1c are described by the equations

$$\frac{\mathrm{d}\theta_\mathrm{A}}{\mathrm{d}\tau} = \xi\frac{\mathrm{d}\psi}{\mathrm{d}\tau} + i_\mathrm{B}(\tau) - \sin\theta_1 - i_2\sin\theta_2 \tag{3}$$

$$\frac{\mathrm{d}^2\tilde{\psi}}{\mathrm{d}\tau^2} + \frac{\omega_\mathrm{L}^2}{\omega_\mathrm{J}^2}\tilde{\psi} \approx \hat{A}_0 i_\mathrm{a.c.}\cos(\hat{\omega}\tau) \tag{4}$$

where $\omega_\mathrm{J} \equiv 2eRI_1/\hbar$, $\tau \equiv \omega_\mathrm{J}t$, $R = R_1R_2/(R_1 + R_2)$, $\xi \equiv (R_1 - R_2)/(R_1 + R_2)$, $\hat{\omega} \equiv \omega/\omega_\mathrm{J}$, $i_\mathrm{B} \equiv I_\mathrm{B}/I_1$, $i_2 \equiv I_2/I_1$ and $\hat{A}_0 \equiv \omega_\mathrm{L}^2R_1/(\omega_\mathrm{J}^2 i_{12}(R_1 + R_2))$. In the remainder, we set $\omega_\mathrm{L}/\omega_\mathrm{J} = 0.005$, $\Gamma_\mathrm{L}/\omega_\mathrm{L} = 7.5\times10^{-5}$, $\hat{A}_0 = 0.0045$, $\xi = -0.6$ and $i_2 = 1.5$.

The dynamics of the SQUID can be obtained starting from equations (3) and (4) for each of the two JJs. In the remainder, we will denote by $X_i^{(j)}$ the quantity X for band i in arm j of the SQUID, see Fig. 1c. We assume the SQUID to be symmetric; the parameters entering the JJs' RCSJ model and the self-inductance L are assumed to be the same for the left and right arm of the SQUID. In experiments, some asymmetry between left and right JJs is expected. We have checked the effect of asymmetries in the SQUID and found that: (1) small asymmetries simply cause the structure of the Shapiro steps to be slightly asymmetric with respect to the biasing current, (2) large asymmetries can give rise to a complicated subharmonic step structure arising from higher harmonic terms and (3) asymmetries alone cannot be responsible for suppression of non-zero even Shapiro steps before entering the Bessel regime. For the kth band, the phase difference $\eta \equiv (\theta_k^{(2)} - \theta_k^{(1)})/2\pi = \hat{\Phi} + \beta(i^{(1)} - i^{(2)})$ where $\hat{\Phi} = \Phi_\mathrm{ext}/\Phi_0$ is the normalized external flux threading the SQUID, $\Phi_0 = h/2e$, $\beta = I_1L/\Phi_0$ and $i^{(j)} = I^{(j)}/I_1$ with $I^{(j)}$ the total current flowing through arm j. Using equations (3) and (4) and considering current conservation and the flux quantization for η, in the limit $\beta \ll 1$, in terms of the phases $\theta_\mathrm{s} \equiv \sum_{ij}\theta_i^{(j)}/4$, $\psi = \psi^{(1)} = \psi^{(2)} = \psi_0 + \tilde{\psi}(t)$, we find (see Supplementary Section 2) that the dynamics of the SQUID are described by the equations

$$\frac{\mathrm{d}\theta_\mathrm{s}}{\mathrm{d}\tau} = \xi\frac{\mathrm{d}\psi}{\mathrm{d}\tau} + \frac{1}{2}\left[i_\mathrm{B} - i_\mathrm{s}(\theta_\mathrm{s}, \psi)\right] \tag{5}$$

$$\begin{aligned} i_\mathrm{s}(\theta_\mathrm{s}, \psi) = {}& 2\cos(\pi\hat{\Phi})\left[\sin(\theta_\mathrm{s} + \psi) + i_2\sin(\theta_\mathrm{s} - \psi)\right] \\ &-2\beta\sin^2(\pi\hat{\Phi})\left[\sin(2(\theta_\mathrm{s} + \psi)) + i_2^2\sin(2(\theta_\mathrm{s} - \psi)) + 2i_2\sin(2\theta_\mathrm{s})\right] \end{aligned} \tag{6}$$

in conjunction with equation (4).

https://doi.org/10.1038/s41567-024-02412-4

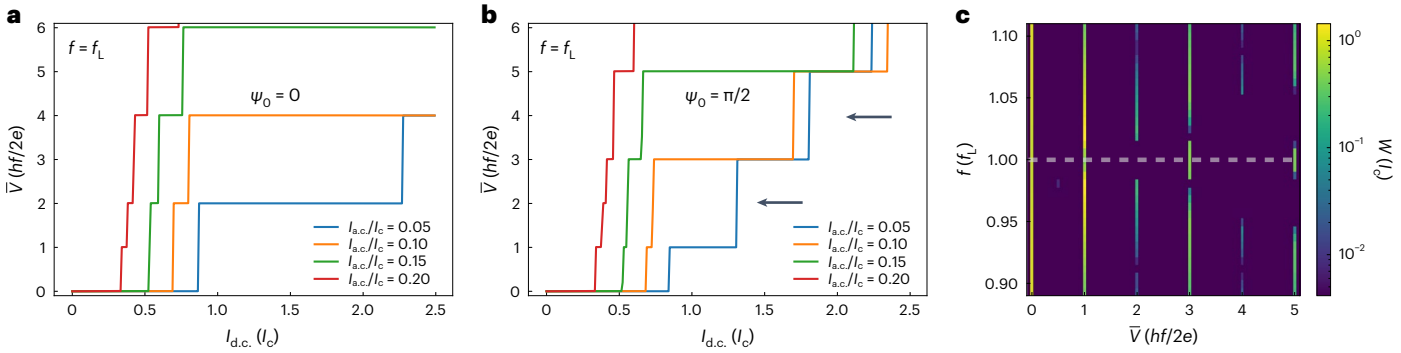

Fig. 2 | Shapiro steps for a SQUID in the presence of a Leggett mode when $\Phi_{ext} = 0$. a,**b**, Simulated V–I curves for the case when $f = f_L$ and $\psi_0 = 0$ (**a**) and $\psi_0 = \pi/2$ (**b**). **c**, Histogram of Shapiro steps as a function of a.c. frequency f with power $I_{a.c.} = 0.05 I_1$. The horizontal dashed line indicates where the a.c. frequency is equal to the Leggett frequency.

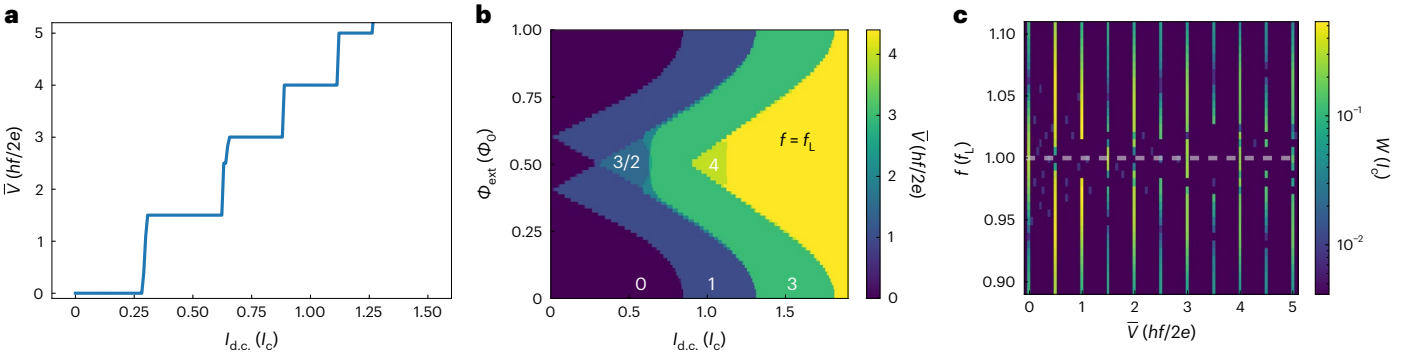

Fig. 3 | Shapiro steps for a SQUID in the presence of a Leggett mode when $\Phi_{ext} \neq 0$. a, Simulated Shapiro steps for a SQUID when $f = f_L$, $I_{a.c.} = 0.05 I_c$ and $\Phi_{ext} = \Phi_0/2$. **b**, Colormap of Shapiro steps as a function of Φ_{ext}. The different steps are labelled in white. **c**, Histogram of Shapiro steps as a function of a.c. frequency f. The horizontal dashed line indicates where the a.c. frequency is equal to the Leggett frequency.

Using equations (4), (5) and (6), we obtain $V_{d.c.} = \bar{V} = \lim_{t_f \to \infty}(1/t_f) \int_0^{t_f} [(\hbar/2e) \mathrm{d}\theta_s/\mathrm{d}t] \mathrm{d}t$ where t_f is the total integration time. Let's first consider $\tilde{\Phi} \bmod 2 = 0$ and set $\beta = 0.05\pi$. For $|\omega - \omega_L| \gg 1$, the dependence of $V_{d.c.}$ with respect to $I_{d.c.}$ exhibits the standard Shapiro steps: all steps are present if either α_1 or α_2 is equal to 1, but only even steps are present if $\alpha_1 = \alpha_2 = 1/2$. For $\omega = \omega_L$, $\psi_0 = 0$ and $\alpha_1 = \alpha_2$, we have that the odd steps are strongly suppressed, see Fig. 2a, so that the structure of the Shapiro steps resembles the structure expected for a topological JJ for which a channel with $\alpha = 1/2$ dominates. However, for $\psi_0 = \pi/2$, and $\alpha_1 = \alpha_2 = 1$, we have the unusual situation that only the even Shapiro steps are suppressed, as shown in Fig. 2b. This behaviour is present as long as $\omega = 2\pi f$ is within the inverse lifetime, Γ_L, of the Leggett mode frequency $f_L = \omega_L/2\pi$. When $\hbar\omega_L = 2\pi\hbar f_L < \Delta_{sc}$ we can expect Γ_L to be quite small. We can calculate the width W of the Shapiro steps by binning the y axis of Fig. 2b for a fixed power. Figure 2c shows the width of the steps, W, as a function of $V_{d.c.}$ and a.c. frequency f, assuming $\Gamma_L = 0.05 f_L$. We see that for $|f - f_L| \ll \Gamma_L$, the even steps are suppressed while the odd steps are strong; we also note that for f far from the resonance, we recover a voltage–current profile in which all the steps are present (apart from small corrections due to higher harmonics).

We can investigate the effect of the Leggett mode on the Shapiro steps when the SQUID is threaded by a non-zero magnetic flux Φ_{ext}. For the case when $\tilde{\Phi} \bmod 2 \neq 0$, we first note that for $\tilde{\Phi} \bmod 2 = 1$, the second term vanishes. In this case, we find that the SQUID's V–I curve exhibits the same Shapiro steps as for the case $\tilde{\Phi} = 0$. When Φ_{ext} is a half-integer of Φ_0, the first term on the right-hand side of equation (6) vanishes and the term proportional to β affects the dynamics of the SQUID. In this case, when $\psi \approx 0$, the factor of 2 in the argument of the sine causes the appearance of half-integer Shapiro steps, as in standard SQUIDs[23] when $\alpha_1 = \alpha_2 = 1$ and the appearance of the odd Shapiro steps when $\alpha_1 = \alpha_2 = 1/2$.

When $f \approx f_L$, so that $\tilde{\psi}$ is not negligible and Φ_{ext} is not a multiple of Φ_0, the SQUID's V–I features are difficult to predict from a simple analysis of the equations. Numerically, for the case when $f = f_L$, $\psi_0 = \pi/2$ and $\Phi_{ext} = \Phi_0/2$, we find that the SQUID has a fairly unique V–I curve, as shown in Fig. 3. Contrary to the case of a single JJ, the odd step at $V = (hf/2e)$ is absent, and a new fractional step at $V = 3/2(hf/2e)$ appears together with a step at $V = 4(hf/2e)$, while the step at $V = 3(hf/2e)$ survives. Figure 3b shows the range of values of Φ_{ext} around $\Phi_0/2$ for which this step structure is present, and Fig. 3c shows how the step structure and the width of the steps depend on the a.c. frequency f, for $f \approx f_L$, when $\Phi_{ext} = \Phi_0/2$.

The discussion above shows that when the equilibrium phase difference, $\psi_0 \bmod 2\pi$, between the two superconducting order parameters is 0, the microwave response of a SQUID in which an undamped Leggett mode is present, for $\omega \approx \omega_L$, is similar to one obtained when the single JJs forming the SQUID have a current–phase relation that is 4π periodic, due either to the presence of a topological superconducting channel or to Landau–Zener processes. The analysis also shows that when $\psi_0 \approx \pi/2$, the SQUID's microwave response, both in the absence and presence of an external magnetic flux Φ_{ext}, exhibits unique qualitative features that cannot be attributed to topological superconducting pairing or Landau–Zener processes.

In a DSM such as Cd_3As_2, the bulk three-dimensional conduction and valence electronic bands touch at isolated points, and a projection of the spectral density onto a surface Brillouin zone reveals Fermi arcs connecting the bulk Dirac points[24,25]. DSMs with proximity-induced superconductivity are predicted to be able to realize exotic non-Abelian

https://doi.org/10.1038/s41567-024-02412-4

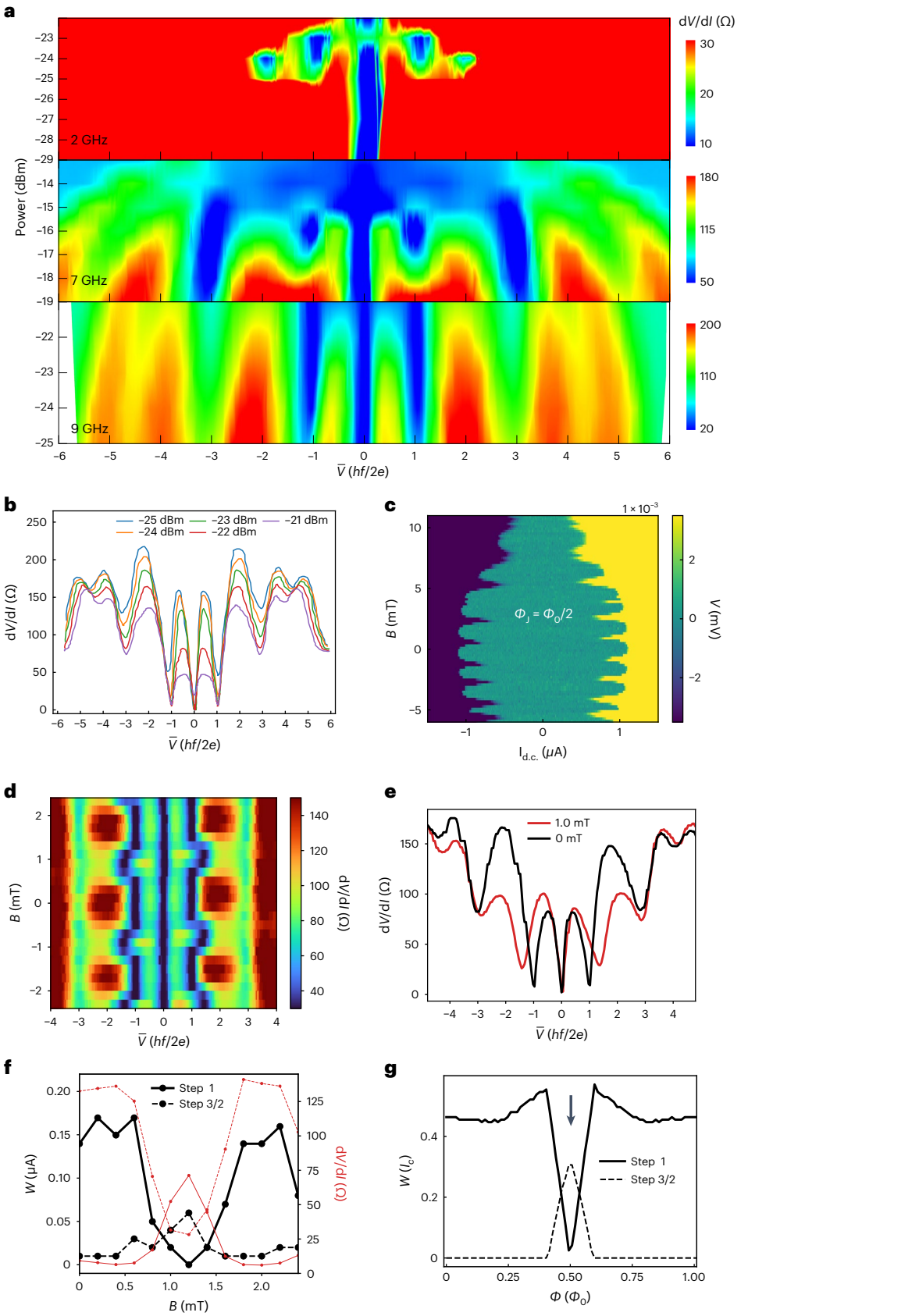

Fig. 4 | Shapiro steps for a SQUID formed by a superconducting Dirac semimetal. a, Experimental differential resistance versus $\bar{V}$ and microwave power at various microwave frequencies with $B = 0$. **b**, Measured differential resistance of the a.c. driven SQUID at various powers, $f = 9$ GHz, and $B = 0$. **c**, Anomalous SQUID oscillations measured in the d.c. regime occurring when the flux $\Phi_J = B \times A_{JJ}$ threading the individual JJs forming the SQUID is a multiple of $\Phi_0/2$. **d**, Colormap of differential resistance versus $\bar{V}$ and B for $f = 9$ GHz and relative power −22 dBm. **e**, Comparison between Shapiro steps (−22 dBm) at zero field and $B = 1$ mT which corresponds to $\Phi_{ext} \approx \Phi_0/2$. **f**, Measured Shapiro step widths (−22 dBm), left vertical axis, and differential resistance, right vertical axis, versus B for $f = 9$ GHz. **g**, Theoretical results for the Shapiro step widths versus flux threading the SQUID at $I_{a.c.} = 0.05 I_c$ and $f = f_L$. The downward arrow points to where the first Shapiro step is suppressed and the 3/2 step is maximized.

anyons that can be used to develop topologically protected qubits[26] and can be used in microwave single-photon detection for sensing applications[27–29]. Another aspect of DSMs that has received less attention in the literature concerns the multiband properties of superconducting DSMs[30–32]. By placing a superconducting material on the surface of Cd_3As_2, superconducting pairing can be induced in the Cd_3As_2 (ref. 30–32). The pairing has been shown to be characterized by two order parameters Δ_1 and Δ_2. Leggett modes result from oscillations of the difference between the phases of the superconducting gaps of different bands, and therefore their presence is always allowed, regardless of the mechanism—intrinsic as in MgB_2, or via proximity effect as in our devices—responsible for the superconducting pairing. In addition, recent experiments on single JJs formed by superconducting leads based on Al/Cd_3As_2 have shown compelling signatures of an equilibrium phase difference $\theta_1 - \theta_2$ between the two phases across the junction, arising from the two superconducting order parameters, being equal to π, implying $\psi_0 = \pi/2$ (ref. 32). Motivated by these results and the theoretical analysis above, we have investigated the microwave response of a SQUID based on Al/Cd_3As_2. Details about the fabrication and measurement of the device can be found in the Methods section and Supplementary Section 5.

At frequency $f = 2$ GHz and $\Phi_{ext} = 0$, the SQUID's measured dV/dI exhibits peaks and valleys consistent with the standard Shapiro steps' structure (Fig. 4a). However, for $f = 7$ GHz and $f = 9$ GHz, for all the microwave powers values considered, the first and third steps are clearly visible, but the second step is strongly suppressed (Fig. 4b). Considering that our device shows no hysteretic features in the current–voltage characteristic and no evidence of a bias-dependent normal resistance, mechanisms for missing Shapiro steps due to hysteresis[33] or bias-dependent resistance[34] are not relevant. When the zeroth step's width approaches zero for $I_{a.c.} \approx I_c$, the system begins to enter the 'Bessel regime', where oscillations in step widths with increasing power $I_{a.c.} > I_c$ regularly occur and can lead to missing steps. Our measurements are not in the Bessel regime, given that for $f \approx 9$ GHz, (1) the zeroth step is clearly non-zero at all powers and (2) the second step is missing at low powers, as shown in Fig. 4a,b (see also Supplementary Fig. 8c) and does not re-appear as the power increases. We find it is very difficult to explain the suppression of even steps at low powers without invoking the presence of a Leggett mode.

We can estimate the value of ω_L in our device, as discussed in Supplementary Section 3. We find that $\omega_L \approx 10$ GHz is quite smaller than the value of $\omega_L \approx 2.3$ THz in MbB_2 (ref. 8), due to the high density of states of the bands of Cd_3As_2. We notice, however, that the precise value of ω_L depends on bands parameters whose accurate estimate is hard to obtain from experiments.

Figure 4c shows the voltage across the SQUID as a function of the perpendicular magnetic field B in the d.c. limit, $I_{a.c.} = 0$. SQUID oscillations of periodicity 1.8 mT are observed, which correspond to an effective SQUID ring area of 1.14 μm^2. Enveloping the SQUID oscillations is the Fraunhofer diffraction pattern of the JJs. Anomalous oscillations can also be observed for B such that the flux threading a single JJ, $\Phi_J = B \times A_{JJ}$, A_{JJ} being the area of the JJ, is a multiple of $\Phi_0/2$. The presence of these oscillations is consistent with a π-periodic supercurrent in each of the JJs forming the SQUID because $\psi_0 = \pi/2$.

In Fig. 4d we present as a colour plot the measured dV/dI as a function of $\bar{V}$ and B in the presence of an a.c. component of the current with $f = 9$ GHz and relative power −22 dBm. Besides the periodicity of the Shapiro steps with respect to B, with a period consistent with the periodicity observed in the d.c. limit, Fig. 4c, we observe interesting features for $B \approx 1$ mT corresponding to $\Phi_{ext} = \Phi_0/2$. To more clearly identify these features, we show in Fig. 4e the dV/dI traces for $B = 0$ mT and $B = 1$ mT. We see that for $B = 1$ mT, that is, $\Phi_{ext} = \Phi_0/2$, both the first and second Shapiro steps are suppressed and a 3/2 subharmonic step emerges, features that are remarkably consistent with the theoretical results shown in Fig. 3. To better understand the evolution of the Shapiro steps' structure with Φ_{ext} when $f = 9$ GHz, in Fig. 4f we plot the measured width of the steps at $V = hf/2e$ and $V = (3/2)(hf/2e)$ as a function of B. We see that when $B \approx 1$ mT, $\Phi_{ext} = \Phi_0/2$, the width of the first step is suppressed, whereas the width of the 3/2 step is enhanced around $B \approx 1$ mT. The evolution of the 1 and 3/2 steps with Φ_{ext} is in good qualitative agreement with the theoretical results, shown in Fig. 4g.

Our theoretical and experimental results show how the response to microwave radiation of JJs and SQUIDs formed by multiband superconductors can be used to identify the presence of Leggett modes in such superconductors. By showing that qualitative signatures in the response due to Leggett modes appear only when the microwave frequency is close to the frequency of the Leggett mode, and when, at equilibrium, the phase difference between superconducting order parameters is not zero, the results also allow experimentally obtaining an estimate of the Leggett mode's frequency and its broadening and of the relative phases between superconducting gaps, all quantities that are otherwise challenging to measure experimentally. When the density of states is large, the energy of the Leggett mode can be well below the superconducting gap making it underdamped and therefore more easily observable and more relevant for the low energy behaviour of the superconductor. This should make our results, and more generally the physics of Leggett modes, relevant for the superconducting states of flat band systems, such as the recently realized twisted bilayers, that in the metallic phase have multiple bands crossing the Fermi energy. Finally, our results suggest that the superconducting state induced in the DSM Cd_3As_2 by the proximity of a standard s-wave superconductor might be characterized by a non-zero difference between the phases of the order parameters[35], making such state very interesting from a fundamental point of view and for possible technological applications.

Online content

Any methods, additional references, Nature Portfolio reporting summaries, source data, extended data, supplementary information, acknowledgements, peer review information; details of author contributions and competing interests; and statements of data and code availability are available at https://doi.org/10.1038/s41567-024-02412-4.

References

1. Tsuda, S. et al. Evidence for a multiple superconducting gap in MgB_2 from high-resolution photoemission spectroscopy. *Phys. Rev. Lett.* **87**, 177006 (2001).
2. Souma, S. et al. The origin of multiple superconducting gaps in MgB_2. *Nature* **423**, 65–67 (2003).
3. Stewart, G. R. Superconductivity in iron compounds. *Rev. Mod. Phys.* **83**, 1589–1652 (2011).
4. Ugeda, M. M. et al. Characterization of collective ground states in single-layer $NbSe_2$. *Nat. Phys.* **12**, 92–97 (2015).
5. Xi, X. et al. Ising pairing in superconducting $NbSe_2$ atomic layers. *Nat. Phys.* **12**, 139–143 (2016).
6. Leggett, A. J. Number-phase fluctuations in two-band superconductors. *Prog. Theor. Phys.* **36**, 901–930 (1966).
7. Brinkman, A. et al. Charge transport in normal metal–magnesiumdiboride junctions. *J. Phys. Chem. Solids* **67**, 407–411 (2006).
8. Blumberg, G. et al. Observation of Leggett's collective mode in a multiband MgB_2 superconductor. *Phys. Rev. Lett.* **99**, 227002 (2007).
9. Klein, M. V. Theory of Raman scattering from Leggett's collective mode in a multiband superconductor: application to MgB_2. *Phys. Rev. B* **82**, 014507 (2010).
10. Mou, D. et al. Strong interaction between electrons and collective excitations in the multiband superconductor MgB_2. *Phys. Rev. B* **91**, 140502 (2015).
11. Giorgianni, F. et al. Leggett mode controlled by light pulses. *Nat. Phys.* **15**, 341–346 (2019).

12. Zhao, S. Z. et al. Observation of soft Leggett mode in superconducting $CaKFe_4As_4$. *Phys. Rev. B* **102**, 144519 (2020).
13. Ota, Y., Machida, M., Koyama, T. & Matsumoto, H. Theory of heterotic superconductor-insulator-superconductor Josephson junctions between single- and multiple-gap superconductors. *Phys. Rev. Lett.* **102**, 237003 (2009).
14. Beenakker, C. W. J. in *Low-Dimensional Electronic Systems* Springer Series in Solid-State Sciences Vol. 111 (eds Bauer, G. et al.) 78–82 (Springer, 1992); https://doi.org/10.1007/978-3-642-84857-5_7
15. Fu, L. & Kane, C. L. Josephson current and noise at a superconductor/quantum-spin-Hall-insulator/superconductor junction. *Phys. Rev. B* **79**, 161408 (2009).
16. Wiedenmann, J. et al. 4π-periodic Josephson supercurrent in HgTe-based topological Josephson junctions. *Nat. Commun.* **7**, 10303 (2016).
17. Dartiailh, M. C. et al. Phase signature of topological transition in Josephson junctions. *Phys. Rev. Lett.* **126**, 036802 (2021).
18. Dartiailh, M. C. et al. Missing Shapiro steps in topologically trivial Josephson junction on InAs quantum well. *Nat. Commun.* **12**, 78 (2021).
19. Shapiro, S. Josephson currents in superconducting tunneling: the effect of microwaves and other observations. *Phys. Rev. Lett.* **11**, 80 (1963).
20. Domínguez, F. et al. Josephson junction dynamics in the presence of 2π and 4π-periodic supercurrents. *Phys. Rev. B* **95**, 195430 (2017).
21. Barone, A. & Paternò, G. *Physics and Applications of the Josephson Effect* (Wiley, 1982); https://onlinelibrary.wiley.com/doi/book/10.1002/352760278X
22. Romeo, F. & De Luca, R. Shapiro steps in symmetric π-SQUIDs. *Physica C* **421**, 35–40 (2005).
23. Vanneste, C. et al. Shapiro steps on current-voltage curves of d.c. SQUIDs. *J. Appl. Phys.* **64**, 242–245 (1988).
24. Wehling, T., Black-Schaffer, A. & Balatsky, A. Dirac materials. *Adv. Phys.* **63**, 1–76 (2014).
25. Armitage, N. P., Mele, E. J. & Vishwanath, A. Weyl and Dirac semimetals in three-dimensional solids. *Rev. Mod. Phys.* **90**, 015001 (2018).
26. Kitaev, A. Y. Unpaired Majorana fermions in quantum wires. *Phys. Usp.* **44**, 131 (2001).
27. Chi, F. et al. Photon-assisted transport through a quantum dot side-coupled to Majorana bound states. *Front. Phys.* **8**, 254 (2020).
28. Chatterjee, E., Pan, W. & Soh, D. Microwave photon number resolving detector using the topological surface state of superconducting cadmium arsenide. *Phys. Rev. Res.* **3**, 023046 (2021).
29. Pan, W., Soh, D., Yu, W., Davids, P. & Nenoff, T. M. Microwave response in a topological superconducting quantum interference device. *Sci. Rep.* **11**, 8615 (2021).
30. Wang, A.-Q. et al. 4π-periodic supercurrent from surface states in Cd_3As_2 nanowire-based Josephson junctions. *Phys. Rev. Lett.* **121**, 237701 (2018).
31. Huang, C. et al. Proximity-induced surface superconductivity in Dirac semimetal Cd_3As_2. *Nat. Commun.* **10**, 2217 (2019).
32. Yu, W. et al. π and 4π Josephson effects mediated by a Dirac semimetal. *Phys. Rev. Lett.* **120**, 177704 (2018).
33. Shelly, C. D., See, P., Rungger, I. & Williams, J. M. Existence of Shapiro steps in the dissipative regime in superconducting weak links. *Phys. Rev. Appl.* **13**, 024070 (2020).
34. Mudi, S. R. & Frolov, S. M. Model for missing Shapiro steps due to bias-dependent resistance. Preprint at https://arxiv.org/abs/2106.00495 (2021).
35. Ng, T. K. & Nagaosa, N. Broken time-reversal symmetry in Josephson junction involving two-band superconductors. *Europhys. Lett.* **87**, 17003 (2009).

Methods

Fabrication

Mechanical exfoliation is used to obtain flat and shiny Cd_3As_2 thin flakes of thickness ~200 nm from an initial bulk ingot material[29], synthesized via a chemical vapour deposition method[36]. The SQUID structure is fabricated by first depositing the Cd_3As_2 thin flake on a Si/SiO_2 substrate with a 1-µm-thick SiO_2 layer. Next, e-beam lithography is used to define 300-nm-thick Al electrodes. Additional details about the device can be found elsewhere[32].

Measurements

To measure the sample resistance, an approximately 11 Hz phase-sensitive lock-in amplifier technique is used with an excitation current of 10 nA. To measure the differential resistance, a large direct current up to ±2 µA is added to the a.c. current. The entire device is immersed in a cryogenic liquid at a temperature of approximately 0.25 K, well below the device's superconducting transition temperature. To measure the microwave response of the device, an Agilent 83592B sweep generator is used to generate microwaves, which are conducted through a semirigid coax cable.

Simulations

The numerical integration of the dynamical equations has been performed using the adaptive Runge–Kutta methods of order four and five.

Data availability

The data that support the findings of this study are publicly available at https://doi.org/10.6084/m9.figshare.24871635 (ref. 37). Source data are provided with this paper.

Code availability

All the codes used to obtain the numerical results presented are available upon reasonable request.

References

36. Ali, M. N. et al. The crystal and electronic structures of Cd_3As_2, the three-dimensional electronic analogue of graphene. *Inorg. Chem.* **53**, 4062–4067 (2014).
37. Cuozzo, J. J. et al. Leggett modes in a Dirac semimetal. *Figshare* https://doi.org/10.6084/m9.figshare.24871635 (2024).

Acknowledgements

This work was supported by the US Department of Energy, Office of Science, Basic Energy Sciences, under Award No. DE-SC0022245 (J.J.C, W.P. and E.R.). J.J.C. also acknowledges support from the Graduate Research Fellowship awarded by the Virginia Space Grant Consortium (VSGC). The authors acknowledge the Cd_3As_2 material synthesis work of D. X. Rademacher and helpful discussions with J. Schirmer. The work at Sandia is supported by a Laboratory Directed Research & Development (LDRD) project. Device fabrication was performed at the Center for Integrated Nanotechnologies, a US Department of Energy (DOE), Office of Basic Energy Sciences (BES), user facility. Sandia National Laboratories is a multimission laboratory managed and operated by National Technology and Engineering Solutions of Sandia LLC, a wholly owned subsidiary of Honeywell International Inc., for the US DOE's National Nuclear Security Administration under contract DE-NA0003525. This paper describes objective technical results and analysis. Any subjective views or opinions that might be expressed in the paper do not necessarily represent the views of the US DOE or the United States Government.

Author contributions

J.J.C. and E.R. developed the theoretical model. J.J.C. carried out the numerical simulations. W.Y., P.D., T.M.N., D.B.S. and W.P. conceived the experiment and contributed to material growth, device fabrication, electronic transport measurements and experimental data analysis. W.P. coordinated the experiment. All authors contributed to interpreting the data. The manuscript was written by J.J.C., W.P. and E.R., with suggestions from all other authors.

Competing interests

The authors declare no competing interests.

Additional information

Supplementary information The online version contains supplementary material available at https://doi.org/10.1038/s41567-024-02412-4.

Correspondence and requests for materials should be addressed to Joseph J. Cuozzo, Wei Pan or Enrico Rossi.

Peer review information *Nature Physics* thanks Alexander Golubov and the other, anonymous, reviewer(s) for their contribution to the peer review of this work.

nature physics

Article

https://doi.org/10.1038/s41567-024-02412-4

Leggett modes in a Dirac semimetal

In the format provided by the authors and unedited

SUPPLEMENTARY INFORMATION

I. DYNAMICS OF A TWO-BANDS JOSEPHSON JUNCTION IN THE PRESENCE OF A LEGGETT MODE

Let's consider a Josephson junction (JJ) where each of the superconducting electrodes are two-band superconductors with phases $\phi_1,\ \phi_2$. Let the intraband phase differences across the junction be $\theta_i = \phi_i^R - \phi_i^L$. To describe the *interband* dynamics in the JJ, we consider the resistively and capacitively shunted junction (RCSJ) model shown in Fig. 1 (d). For the ac Josephson effect we have that the voltage V across a weak link, denoted by crosses in Fig. 1 (d), is given by $V = \hbar\dot{\varphi}_i/2e$, where φ is the phase difference across the weak link of the superconducting order parameters. Let $\phi_L = \phi_1^L - \phi_2^L$, $\phi_R = \phi_1^R - \psi_2^R$ and $\theta_i = \phi_i^R - \phi_i^L$. From Kirchhoff's voltage law applied to the loop formed by the weak links in Fig. 1 (d) we obtain

$$\dot{\phi}_L + \dot{\theta}_2 - \dot{\phi}_R - \dot{\theta}_1 = 0 \tag{S1}$$

and then $\dot{\theta}_2 - \dot{\theta}_1 = \dot{\phi}_R - \dot{\phi}_L$.

Let I_{12}^L, I_{12}^R be the interband critical dc Josephson current on the left side and right side, respectively, of the circuit shown in Fig. 1 (d) of the main text, and C_{12}^L, C_{12}^R the left-side, right-side, interband capacitances. From charge conservation we obtain

$$I_{12}^L \sin\phi_L + \frac{\hbar}{2e} C_{12}^L \ddot{\phi}^L = I_2 \sin\theta_2 + \frac{\hbar}{2eR_2}\dot{\theta}_2 \tag{S2}$$

$$I_{12}^R \sin\phi_R + \frac{\hbar}{2e} C_{12}^R \ddot{\phi}^R = -(I_2 \sin\theta_2 + \frac{\hbar}{2eR_2}\dot{\theta}_2) \tag{S3}$$

If we assume $C_{12}^L = C_{12}^R \equiv C_{12}$ and $I_{12}^L = I_{12}^R \equiv I_{12}$, it is clear that $\phi_R = -\phi_L$. Then, from Eq. (S1) we obtain

$$\psi \equiv \frac{\theta_1 - \theta_2}{2} = \phi_L = -\phi_R. \tag{S4}$$

Equation (S4) establishes the direct relation between phases across the Josephson junction, θ_i, and the phases ϕ_R, ϕ_L, characterizing the Leggett modes in the two superconducting leads. In particular Eq. (S4) implies that the dynamics of the Leggett modes will in general affect the dynamics of the phases across the JJ.

We now obtain the dynamics of the current biased JJ shown in Fig. 1 (d) taking into account the presence of a Leggett mode. When a bias current I_B is applied across the junction, charge conservation gives

$$I_B = I_1 \sin\theta_1 + I_2 \sin\theta_2 + \frac{V_1}{R_1} + \frac{V_2}{R_2} \tag{S5}$$

where I_i is the critical Josephson current for the i^{th} band and V_i/R_i is the current through the resistive channel in the i^{th} band. Let $\theta_A \equiv (\theta_1 + \theta_2)/2$. Considering Eq. (S4), we can write $\theta_1 = \theta_A + \psi$, $\theta_2 = \theta_A - \psi$ and then

$$I_B = I_1 \sin\theta_1 + I_2 \sin\theta_2 + \frac{\hbar}{2eR}\left(\dot{\theta}_A - \xi\dot{\psi}\right) \tag{S6}$$

where $R = R_1R_2/(R_1+R_2)$ is the parallel resistance of the resistors R_1 and R_2, $\xi = (R_1 - R_2)/(R_1 + R_2)$ quantifies the asymmetry in resistance between the bands. Defining $\omega_J \equiv 2eRI_1/\hbar$, $\tau \equiv \omega_J t$, we can write Eq. (S6) as

$$\frac{d\theta_A}{d\tau} = \xi\frac{d\psi}{d\tau} + i_B - \sin\theta_1 - i_2\sin\theta_2 \tag{S7}$$

where currents have been normalized with respect to I_1: $i_B = I_B/I_1$ and $i_2 = I_2/I_1$. Equation (S7) is the key equation to describe the behavior of the 2-band JJ, and SQUID (see next section), in the presence of a Leggett mode. The key modification due to the Leggett mode is the term $\xi d\psi/d\tau$. The evolution in time of $\psi(t)$ depends on several microscopic details that are beyond the level of the effective description used here. We have assumed $\psi(t)$ to follow the dynamics of a harmonic oscillator driven by a periodic term due to the microwave radiation. Below we show that, in first approximation, this simplified evolution is also consistent with the RSCJ model shown in Fig. 1 (d).

We can rewrite Eq. (S3) in the form:

$$\frac{d^2\psi}{d\tau^2} + \frac{R\omega_L^2}{\omega_J^2 i_{12}(R_1+R_2)}\frac{d\psi}{d\tau} + \frac{\omega_L^2}{\omega_J^2}\sin\psi = \frac{\omega_L^2 R_1}{\omega_J^2 i_{i2}(R_1+R_2)}\left[i_B + (R_2/R_1)i_2\sin(\theta_A - \psi) - \sin(\theta_A + \psi)\right]. \tag{S8}$$

where $i_{12} \equiv I_{12}/I_1$, $\omega_L = \sqrt{(2e/\hbar)I_{12}/C_{12}}$ is the Leggett mode's frequency, and $i_B = i_{dc} + i_{ac}\cos(\omega\tau)$ Equations (S7) and (S8) completely define the dynamics of the two-bands JJ described by the effective RCSJ circuit shown in Fig. 1 (d). Eq. (S8) is equivalent to the equation for a damped, driven, oscillator; the right hand side of the equation being the driving term. To qualitatively understand the effect of a resonant Leggett mode, in first approximation, we can neglect the damping term proportional $d\psi/d\tau$, and the term $i_{dc} + (R_2/R_1)i_2\sin(\theta_A - \psi) - \sin(\theta_A + \psi)$ on the right hand side of the equation. Then by linearizing the $\sin\psi$ around the equilibrium value ψ_0 for $\tilde{\psi} \equiv \psi - \psi_0$ we obtain the simple equation

$$\frac{d^2\tilde{\psi}}{d\tau^2} + \frac{\omega_L^2}{\omega_J^2}\tilde{\psi} = \frac{\omega_L^2 R_1}{\omega_J^2 i_{i2}(R_1+R_2)} i_{ac}\cos(\hat{\omega}\tau) \tag{S9}$$

describing a harmonic oscillator periodically driven by a force of amplitude $\hat{A}_0 i_{ac}$, with $\hat{A}_0 \equiv \omega_L^2 R_1/(\omega_J^2 i_{12}(R_1+R_2))$. Here $\hat{\omega} \equiv \omega/\omega_J$. In our calculations the effect of the damping term is taken into account by considering a finite broadening, Γ_L, of the Leggett mode's resonance frequency.

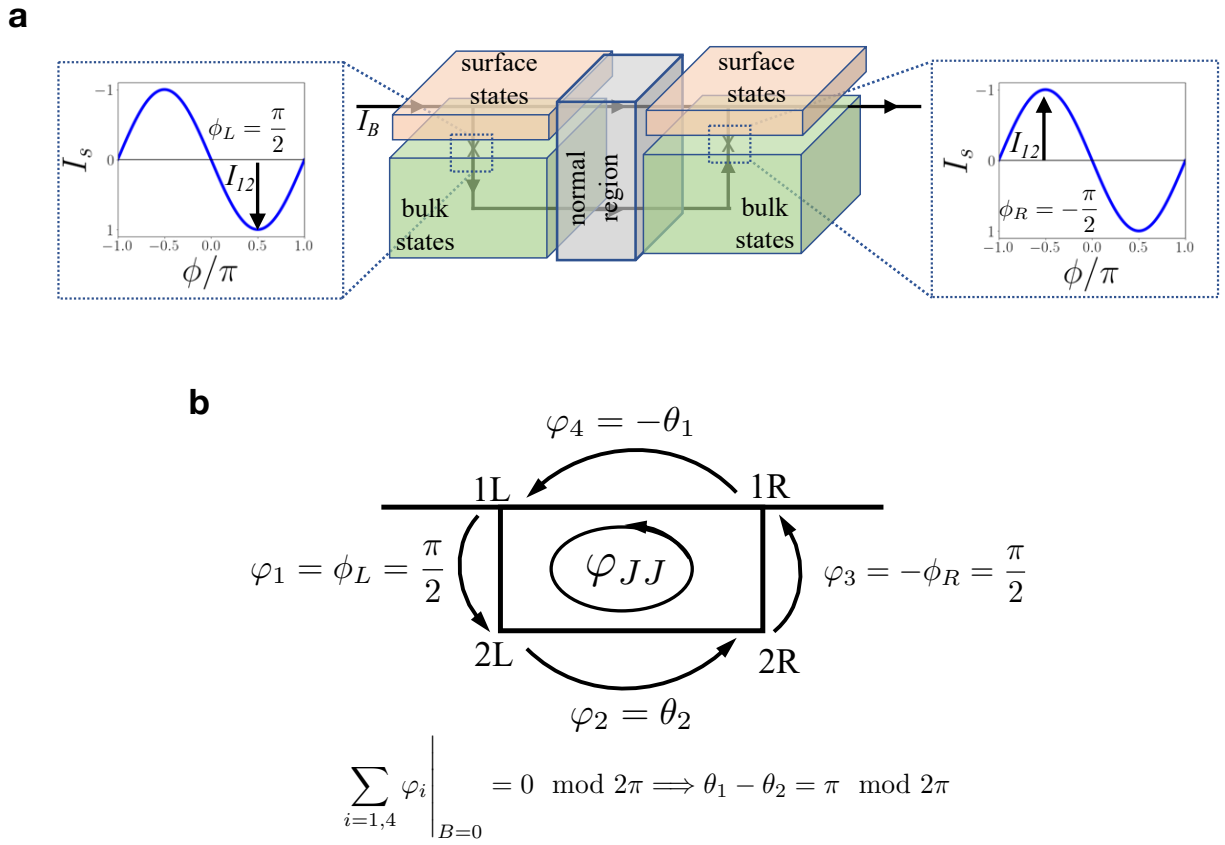

Figure S1. **a** Schematic currents across a JJ based on a DSM. **b** Schematic of phases across a JJ based on a DSM.

In this model the current flows into the bulk of the DSM only via the surface states, as shown by the schematic circuit of Fig. 1(d). The lowest energy path for the current to flow into the bulk is via a Josephson supercurrent, I_s, between the surface band and the bulk band. Considering that in general $I_s \propto \sin\varphi$, where φ is the difference between the phases of the superconducting order parameters, we see that to maximize the supercurrent between surface and bulk the system will self-tune in a state for which $\phi \approx \pi/2$ on the left lead, and $\phi \approx -\pi/2$ on the right lead, given that in the left lead the interband current (I_{12}) flows from surface to bulk and in the right lead it flows from bulk to surface, see Fig S1 (a). Another possibility is that finite phase differences, $\phi \approx \pi/2$ on the left and $\phi \approx -\pi/2$ on the right (or vice-versa), between bands 1 and 2 might arise due to the establishment of time-reversal broken symmetry states as suggested in Ref.[1].

The presence of interband phase differences approximately equal to $\pm\pi/2$ is also consistent with the anomalous behavior in the dc response of the SQUID that we present in Fig. 4 (b). As for the case of a single JJ [2], the SQUID's response in the dc limit can be attributed to a π-phase overall difference between the two effective channels connecting the left and right leads, see Fig. S1 (b).

II. DYNAMICS OF A SQUID FORMED BY TWO-BANDS SUPERCONDUCTING LEADS AND IN THE PRESENCE OF A LEGGETT MODE.

In this section we derive the equations that we use to simulate the dynamics of a two-bands SQUID in presence of a resonant Leggett mode. We assume the SQUID to be symmetric:

$$C_{12}^{(1)} = C_{12}^{(2)} \equiv C_{12}; \quad R_i^{(1)} = R_i^{(2)} \equiv R_i; \quad I_i^{(1)} = I_i^{(2)} \equiv J_i;$$
$$I_{12}^{(1)} = I_{21}^{(1)} = I_{12}^{(2)} = I_{21}^{(2)} \equiv I_{12},$$

where $X_i^{(j)}$ denotes quantity X in band i, and arm (j) of the SQUID. Normalizing as usual the currents with I_1, from charge conservation and magnetic flux quantization we have:

$$i^{(1)} + i^{(2)} = i_B \tag{S10}$$

$$i^{(1)} - i^{(2)} = \frac{\theta_i^{(2)} - \theta_i^{(1)}}{2\pi\beta} - \frac{\hat{\Phi}}{\beta} + \frac{m}{\beta} \tag{S11}$$

where $\beta \equiv I_1 L/\Phi_0$, $\hat{\Phi} \equiv \Phi_{ext}/\Phi_0$, and m is an integer that without loss of generality we can set equal to zero. For the total current in arm (j) we have:

$$i^{(j)} = \frac{\hbar}{2eR_1 I_1}\frac{d\theta_1^{(j)}}{dt} + \frac{\hbar}{2eR_2 I_1}\frac{d\theta_2^{(j)}}{dt} + \sin(\theta_1^{(j)}) + i_2^{(j)}\sin(\theta_2^{(j)}). \tag{S12}$$

Let's now define

$$\psi^{(1)} \equiv \frac{\theta_1^{(1)} - \theta_2^{(1)}}{2}; \quad \psi^{(2)} \equiv \frac{\theta_1^{(2)} - \theta_2^{(2)}}{2}; \quad \eta_1 \equiv \frac{\theta_1^{(2)} - \theta_1^{(1)}}{2\pi}; \quad \eta_2 \equiv \frac{\theta_2^{(2)} - \theta_2^{(1)}}{2\pi}; \quad \theta_s = \frac{1}{4}\sum_{ij}\theta_i^{(j)}. \tag{S13}$$

Because the flux quantization condition is the same for both bands, we have $\eta_1 = \eta_2 \equiv \eta$, and $\psi^{(1)} = \psi^{(2)} \equiv \psi$. ψ is the phase associated to the Leggett mode and its dynamics is given by Eq. (S9). By using Eq. (S12) to express $i^{(j)}$ in Eqs. (S10), (S11) we obtain the following dynamical equations for θ_s and η

$$\frac{d\theta_s}{d\tau} - \xi\frac{d\psi}{d\tau} = \frac{i_B}{2} - \frac{1}{2}i_s(\theta_s, \psi, \eta) \tag{S14}$$

$$2\pi\frac{d\eta}{d\tau} = -\frac{\eta}{\beta} + \frac{\hat{\Phi}}{\beta} + i_d(\theta_s, \psi, \eta) \tag{S15}$$

where

$$\begin{aligned} i_s(\theta_s, \psi, \eta) &= \sin\theta_1^{(1)} + \sin\theta_1^{(2)} + i_2[\sin\theta_2^{(1)} + \sin\theta_2^{(2)}] \\ &= \sin(\theta_s + \psi - \pi\eta) + \sin(\theta_s + \psi + \pi\eta) + i_2[\sin(\theta_s - \psi - \pi\eta) + \sin(\theta_s - \psi + \pi\eta)]; \end{aligned} \tag{S16}$$

$$\begin{aligned} i_d(\theta_s, \psi, \eta) &= \sin\theta_1^{(1)} - \sin\theta_1^{(2)} + i_2[\sin\theta_2^{(1)} - \sin\theta_2^{(2)}] \\ &= \sin(\theta_s + \psi - \pi\eta) - \sin(\theta_s + \psi + \pi\eta) + i_2[\sin(\theta_s - \psi - \pi\eta) - \sin(\theta_s - \psi + \pi\eta)] \end{aligned} \tag{S17}$$

i_s is the supercurrent fraction of the total current across the SQUID. In the limit $\beta \ll 1$ we can assume[4]

$$\eta = \hat{\Phi} + \beta\tilde{\eta} + \mathcal{O}(\beta^2). \tag{S18}$$

From Eq. (S15), for $\tilde{\eta}$, we find:

$$\tilde{\eta} = 2\sin(\pi\hat{\Phi})[\cos(\theta_s + \psi) + i_2\cos(\theta_s - \psi)] + \mathcal{O}(\beta)] \tag{S19}$$

Replacing in the equation (S16) for i_s the expression for η obtained by combining Eqs. (S18), (S19), we obtain, to linear order in β:

$$\begin{aligned} i_s(\theta_s, \psi) =& 2\cos(\pi\hat{\Phi})[\sin(\theta_s + \psi) + i_2\sin(\theta_s - \psi)] - \\ & 2\beta\sin^2(\pi\hat{\Phi})[\sin(2(\theta_s + \psi)) + i_2^2\sin(2(\theta_s - \psi)) + 2i_2\sin(2\theta_s)]. \end{aligned} \tag{S20}$$

Notice that up to linear order in β i_s only depends on θ_s and ψ.

Equations (S14), (S20), and (S9) completely determine the dynamics of the SQUID. To numerically integrate these non-linear differential equations we used an adaptive fourth-order Runge-Kutta method. The parameters of the model used in the simulations are given in Table I.

ω_L/ω_J	Γ_L/ω_L	$\hat{A}$	ξ	i_2	β
0.005	$7.5 \cdot 10^{-5}$	$4.5 \cdot 10^{-3}$	-0.6	1.5	0.05π

TABLE I.

III. ESTIMATION OF ω_L

We can estimate the value of $\omega_L = \sqrt{\frac{2eI_{12}}{\hbar C_{12}}}$ in our device by considering that in the experiment the critical current $I_c \approx 1\mu$A so that $I_{12} \approx 1.5I_c/(1+1.5) = 0.6$ μA, and estimating the interband capacitance C_{12} given by the the quantum capacitances (C_1, C_2) in series of the two bands: $1/C_{12} = 1/C_1 + 1/C_2$. $C_i = e^2\nu_i$ with ν_i the density of states of band i. For surface states, assuming a quadratic dispersion $\epsilon_k \approx \frac{\hbar^2}{2m*}k^2$, we obtain $\nu_1 = \frac{L_xL_y}{\pi}\frac{m^*}{\hbar^2}$ where m^* is the effective mass and L_xL_y is the area of proximitized Dirac semimetal. For bulk states, assuming a linear dispersion $\epsilon_k \approx \hbar v_F k$, we have $\nu_2 = \frac{L_xL_yL_z}{\pi^2}\frac{\epsilon_F^2}{(\hbar v_F)^3}$ where L_z is the sample's thickness. We have $m^* \approx 0.8m_e$ [5] and $L_xL_y \approx 1$ μm^2 so that $\nu_1 \approx 3.2 \times 10^3$ meV^{-1}. Considering that $L_z \approx 200$ nm, $\hbar v_F \approx 0.3$ meV$\cdot\mu$m[6,7], and $\epsilon_F \approx 200$ meV, we find $\nu_2 \approx 2 \times 10^4$ meV^{-1}. We then obtain $C_{12}^{-1} = \frac{1}{e^2}\left(\frac{\nu_1+\nu_2}{\nu_1\nu_2}\right) \approx \frac{1}{e^2\nu_1}$ since $\nu_1 \ll \nu_1$, and, finally, $\omega_L \approx 10$ GHz, remarkably close to the value for which experimentally the suppression of the even Shapiro steps is stronger.

IV. ADDITIONAL THEORETICAL RESULTS

In Fig. S2 we present additional numerical VI curves in the case where $\psi_0 = 0$. Here, we see, as mentioned in the main text, the missing steps are odd integer multiples of $(hf/2e)$. The ac frequency range in Fig. S2a-d is chosen to cover the approximate half-width of the Leggett mode resonance in the amplitude $A_\omega = A_0\Gamma_L\omega/((\omega^2-\omega_L^2)^2+\Gamma_L^2\omega^2)$, illustrating the robustness of the missing steps over a bandwidth proportional to the inverse lifetime of the Leggett mode.

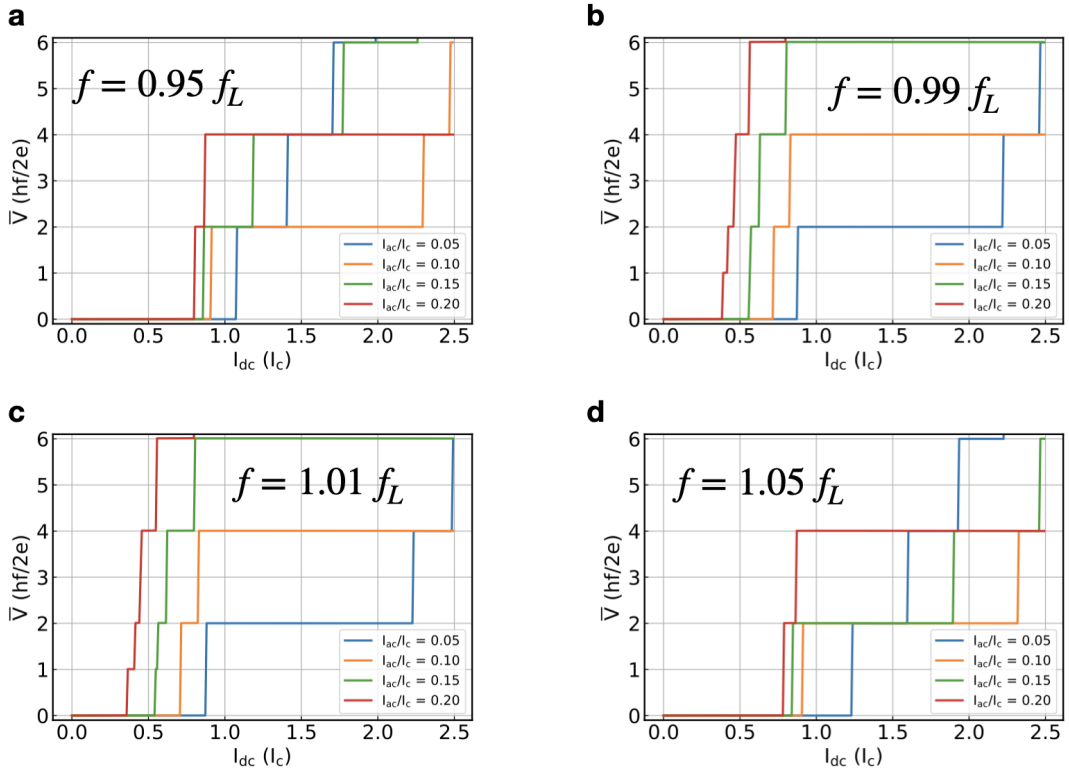

Figure S2. Shapiro steps at various ac frequencies for $\Phi = 0$ and using the same parameters as those used to generate other calculations except that here the intrinsic phase between the two bands in a given junction is zero (rather than π).

In Fig. S3, we present calculations of Shapiro step widths of the n^{th} step corresponding to $\overline{V} = n(hf/2e)$ in the case where $\psi_0 = \pi/2$. Fig. S3a-b show the step width ac frequency dependence near the Leggett mode frequency and for $\hat{\Phi} = 0$ and $I_{ac}/I_c = 0.05$, where a normalized A_ω is shown in black for reference. Clearly, deviations from the conventional Shapiro step dependence follows the resonant Leggett amplitude. Fig. S3c show the power dependence of steps for $\hat{\Phi} = 0$ and $f = f_L$. We see the gap is suppressed at $I_{ac} \approx 0.25\ I_c$, which is much smaller than expected in the conventional case. Furthermore, the step width dependence of odd steps exhibit resonant features appearing consecutively with increasing power and disappering with the gap closure. Once the gap is closed, step widths exhibit oscillations in power, similar to the conventional Bessel regime.

In Fig. S3d-e, we show the step width ac frequency dependence near the Leggett mode frequency and for $\hat{\Phi} = 1/2$ and $I_{ac}/I_c = 0.05$, where a normalized A_ω is shown in black for reference. We observe a weakening of the gap near the Leggett frequency, similar to the zero-flux case, but the gap actually becomes enhanced at the Leggett frequency. In Fig. S3f, we present the power dependence of steps for $\hat{\Phi} = 1/2$ and $f = f_L$. We find similar resonant behavior of odd steps at low power, but the features are difficult to distinguish between oscillations at higher powers associated with the typical Bessel oscillations.

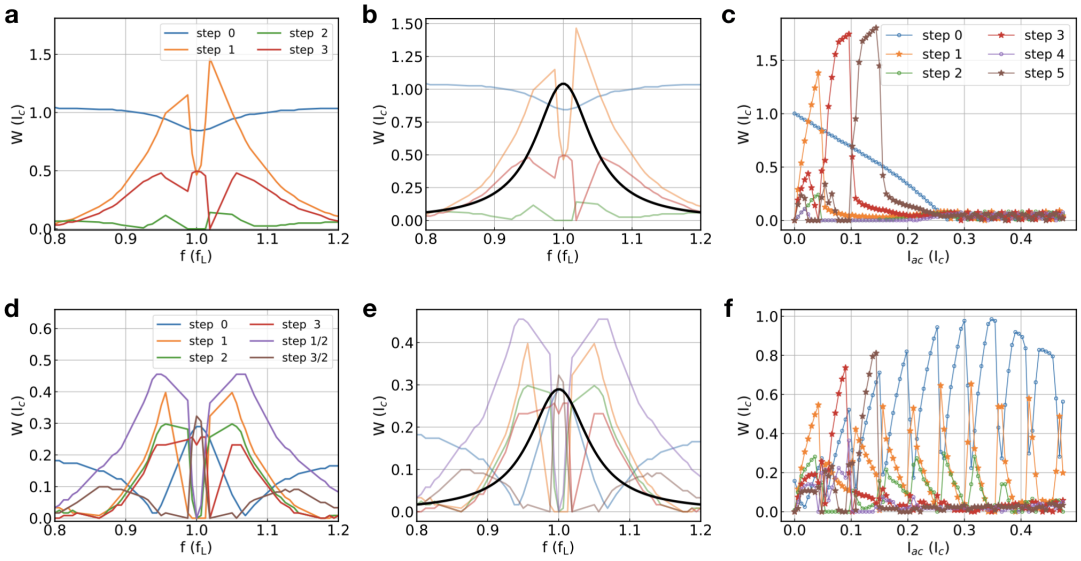

Figure S3. **a-b** Step width dependence on ac frequency for $\Phi = 0$ and $I_{ac} = 0.05 I_c$. The bold black line represents the Lorenzian corresponding to the Leggett mode linewidth. **c** Step width dependence on ac power for $\Phi = 0$ and $f = f_L$. **d-e** Step widths dependence on ac frequency for $\Phi = \Phi_0/2$ and $I_{ac} = 0.05 I_c$. **f** Step width dependence on ac power for $\Phi = \Phi_0/2$ and $f = f_L$.

We can increase bandwidth to include 7 GHz assuming $f_L \approx 9$ GHz by decreasing the lifetime of the Leggett mode in our simulations (i.e. increasing Γ_L by a factor of 10). The results are shown in Fig. S4. The bandwidth where odd steps are enhanced and even steps are suppressed has increased, but even steps are not completely suppressed. In reality, thermal fluctuations may wash out such weak even steps.

V. EFFECT OF THERMAL FLUCTUATIONS

At low temperatures hysteresis effects can give rise to trivial missing steps[3]. To show that thermal fluctuations are responsible for the smearing of the Shapiro steps we have considered a model in which their effect is included via a fluctuating noise current in the RSJ model[8]:

$$I_c \sin(\phi) + \frac{\hbar}{2eR}\frac{d\phi}{dt} = I_{bias} + I_c \rho(T,t) \tag{S21}$$

$$\langle \rho \rangle = 0, \quad \langle \rho(t)\rho(t') \rangle = \frac{2k_B T}{eI_c R}\delta(t-t'). \tag{S22}$$

Using parameters similar to the ones for our device we have obtained results like the ones shown in Fig. (S5): the left panel shows results for the case $T = 0$, and the right panel the results for the case when $T \approx 750$ mK. We can see that

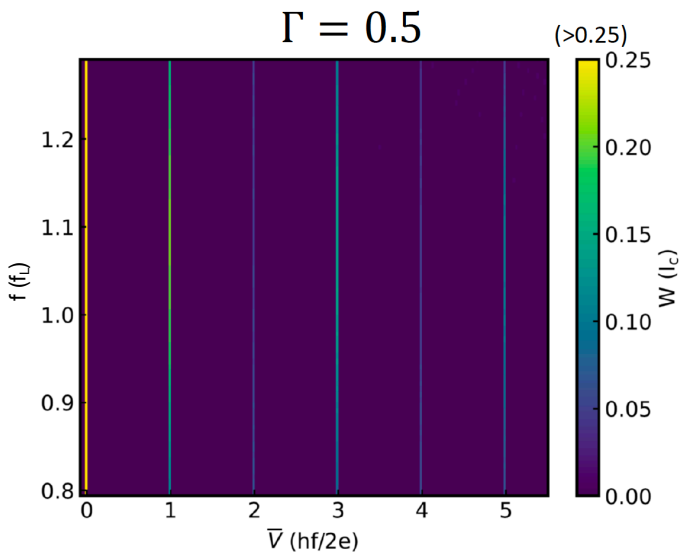

Figure S4. Shapiro step width W as a function of microwave frequency f and $\bar{V}$ near the Leggett frequency with $\Gamma = 0.5$.

thermal effects smear the Shapiro steps and the resistance of Shapiro steps tends to increase with voltage. Notice that even though thermal fluctuations suppress the steps, and therefore the dips of the dV/dI curve, even at the relative large temperature of 750 mK, they do not convert a dip into a maximum. For this reason thermal fluctuations are extremely unlikely to be the cause of the peaks that we observe for $V = 2(hf/2e)$ in the experimental dV/dI profiles.

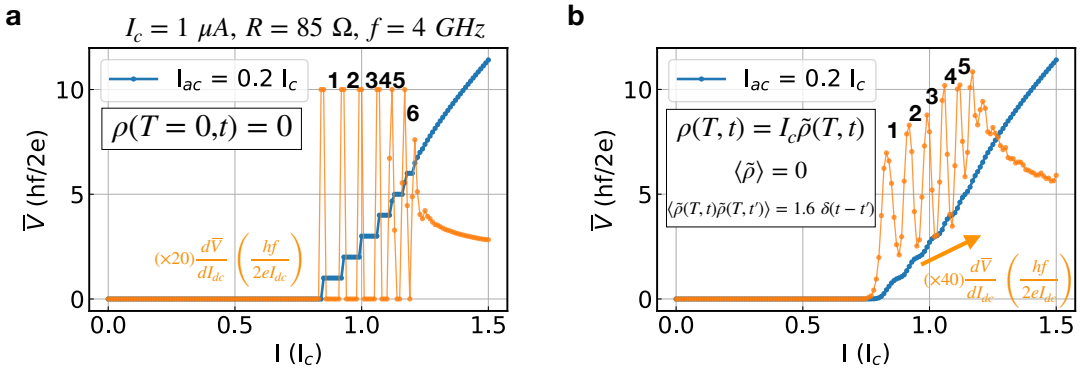

Figure S5. Illustrate thermal fluctuation effects on Shapiro steps.

VI. DEVICE CHARACTERIZATION

Fig. S6a shows an SEM image of the SQUID device used in the experiment. The scale bar is 5 μm. For each Josephson junction in the SQUID, the width is 600 nm, and the gap 150 nm. The size of the middle open square is about 800nm x 800nm. For IV and differential resistance measurements, the ac/dc current runs from contact 1 to contact 3. The dc/ac voltage is measured between contacts 2 and 4. In Fig. S6b, we present the I-V curve measured at B = 0T. The critical current is $\sim 1.1\ \mu A$. In Fig. S6c, we show I-V curves as a function of out-of-plane magnetic fields, at a higher temperature of T = 0.39K (compared to Fig. 4a in the main text). In this plot, red color represents positive Vdc, blue negative Vdc. In the green color regime, Vdc = 0. A typical feature, i.e., the envelop of the SQUID oscillatory pattern being modulated by the Fraunhofer diffraction pattern of the single Josephson junction, is clearly seen.

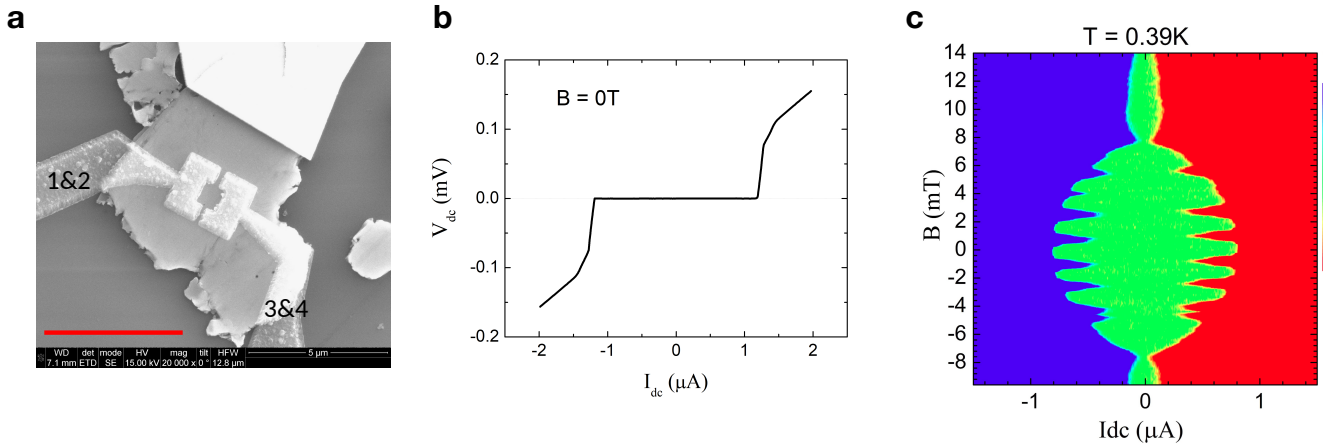

Figure S6. **a** An SEM image of the SQUID device used in the experiment. **b** The I-V curve measured at B = 0T. **c** The I-V curves as a function of out-of-plane magnetic fields, at a higher temperature of T = 0.39K.

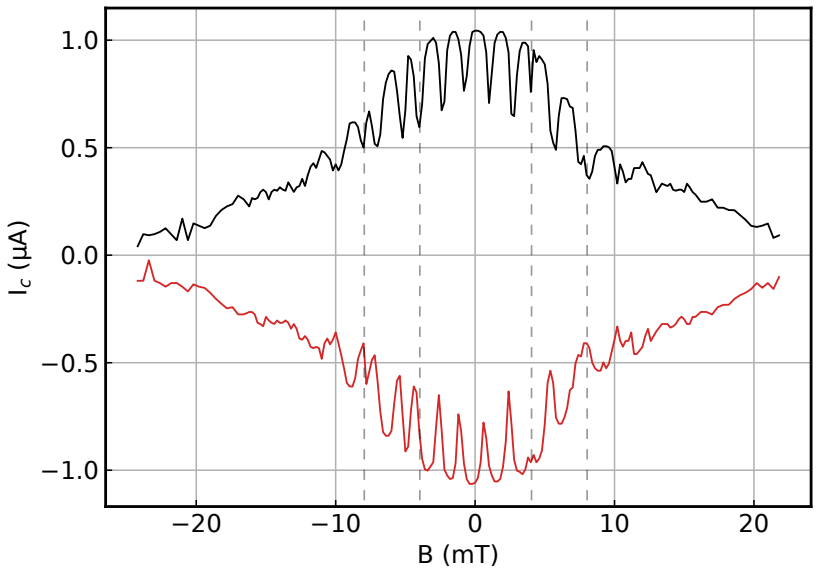

Figure S7. Measured critical currents for positive and negative current biases where dashed lines correspond to the dashed lines in Fig. 4c.

VII. ADDITIONAL EXPERIMENTAL RESULTS

In Fig. S8 we present additional measurements of dV/dI and VI curves at zero magnetic field. In Fig. S8a, we show the differential resistance at 2 GHz for various microwave powers. We see that steps 0, ± 1, ± 2 are clearly observed before dissipative effects wash out higher steps. The measured VI curves are shown in Fig. S8b, where the steps are not easily resolved with the naked eye (hence, the need for dV/dI measurements). Fig. S8c shows VI curves at 9 GHz, showing a large first steps, the clear suppression of the second step, and a weak third step.

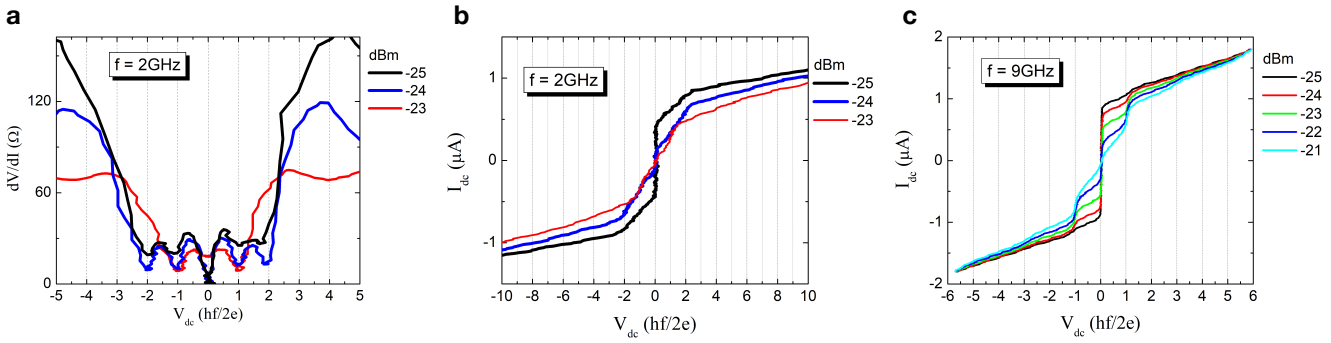

Figure S8. **a** The differential resistance at 2 GHz for a few microwave power levels. At this low frequency, both even and odd Shapiro steps are seen. **b** The corresponding I-V curves at 2 GHz. **c** The I-V curves at 9GHz. The even Shapiro steps are suppressed, as shown in the differential resistance in Fig. 4 of the main text.

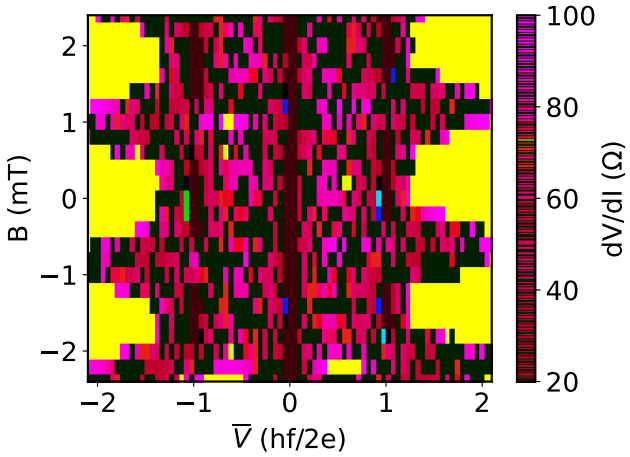

Figure S9. Magnetic field response data from Fig. 4 (c) where a smaller range of dV/dI and a more dynamic colorbar are used to illustrate the discontinuous jump between 1 and 3/2 steps.

REFERENCES

[1] T. K. Ng and N. Nagaosa, Broken time-reversal symmetry in Josephson junction involving two-band superconductors, Europhysics Letters **87**, 17003 (2009).

[2] W. Yu, W. Pan, D. L. Medlin, M. A. Rodriguez, S. R. Lee, Z. Q. Bao, and F. Zhang, π and 4π Josephson Effects Mediated by a Dirac Semimetal, Phys. Rev. Lett. **120**, 177704 (2018).

[3] M. C. Dartiailh, J. J. Cuozzo, B. H. Elfeky, W. Mayer, J. Yuan, K. S. Wickramasinghe, E. Rossi, and J. Shabani, Missing Shapiro steps in topologically trivial Josephson junction on InAs quantum well, Nature Communications **12**, 78 (2021).

[4] F. Romeo and R. De Luca, Shapiro steps in symmetric π-SQUID's, Physica C: Superconductivity **421**, 35 (2005).

[5] A. Chen, D. I. Pikulin, and M. Franz, Josephson current signatures of Majorana flat bands on the surface of time-reversal-invariant Weyl and Dirac semimetals, Phys. Rev. B **95**, 174505 (2017).

[6] Z. Wang, H. Weng, Q. Wu, X. Dai, and Z. Fang, Three-dimensional Dirac semimetal and quantum transport in Cd_3As_2, Phys. Rev. B **88**, 125427 (2013).
[7] S. Borisenko, Q. Gibson, D. Evtushinsky, V. Zabolotnyy, B. Büchner, and R. Cava, Experimental Realization of a Three-Dimensional Dirac Semimetal, Phys. Rev. Lett. **113**, 027603 (2014).
[8] C. M. Falco, W. H. Parker, S. E. Trullinger, and P. K. Hansma, Effect of thermal noise on current-voltage characteristics of Josephson junctions, Phys. Rev. B **10**, 1103 (1974).